



Investigation of packed conductive foams as a novel reactor configuration for methane steam reforming

Riccardo Balzarotti, Matteo Ambrosetti, Alessandra Beretta, Gianpiero Groppi, Enrico Tronconi*

Politecnico di Milano, Dipartimento di Energia, Via La Masa 34, 20156 Milano, Italy

HIGHLIGHTS

- Packed foams successfully applied to SMR process.
- Systematic increase of productivity noted at fixed oven temperature.
- Foam conductivity enhances heat transfer properties.
- Development of a heat transfer model for packed foams.

ARTICLE INFO

Keywords:

Process intensification
Steam reforming
Heat transfer
Metallic foams
Packed foams

ABSTRACT

In this work, a novel fixed bed reactor configuration is proposed and tested for the steam reforming of methane; the proposed solution consists of filling the voids of highly conductive metallic open-cell foams with small catalytic pellets. This reactor layout aims at enhancing the radial heat transfer of the tubular reactor by exploiting the thermal conductivity of the solid interconnected matrix, while keeping a target catalyst inventory and avoiding issues related to washcoating of metallic structures.

Tests were performed using a Rh/Al₂O₃ catalyst in the form of alumina egg-shell particles, with diameter of 600 μm. FeCrAlY open cell foams of 12 PPI and copper open cell foams of 10 and 40 PPI were compared to a conventional packed bed system; experiments were performed at GHSV of 5000 and 10000 h⁻¹ at oven temperatures in the 600–800 °C range. Experiments demonstrated a benefit in terms of the thermal management of the reactor and an increase of productivity at the same furnace temperature in kinetically-limited conditions. A heat transfer model of the packed foams was developed based on the approach of electric equivalent circuit; the model incorporates independently estimated lumped or effective parameters and provides an engineering rationale of the observed reduction of temperature gradients across the catalytic bed.

1. Introduction

Hydrogen and syngas are very important energy and chemical commodities; they are mainly produced by steam reforming of natural gas and light hydrocarbons due to the cost effectiveness of the technology [1]. Externally heated multi-tubular packed bed reactor layouts are commonly applied, where a convective heat transfer mechanism is exploited and optimized to supply the heat for the reaction by running the process at high flow rate, thus at the large production scale [2]. However, there is an increasing demand for distributed hydrogen and syngas production, which calls for clean, sustainable, and cost-competitive production processes [3,4]. The latter is an emerging engineering research topic, as new solutions to downsize the reactors are required, as well as to design compact, reliable, flexible and modular systems,

capable of fast responses to variable hydrogen demands [5].

Among the short-term options for the small-scale production of hydrogen, the steam reforming of natural gas (MSR: Methane Steam Reforming) is one of the most interesting solutions, made highly reliable by the industrial experience and the existing infrastructures. Nevertheless, many R&D needs are present, being the scale down of large industrial reformers a challenging task, as it calls for the intensification of the process [6]: the highly endothermic nature of the reaction would induce heat transfer limitations [7], especially at the low flow rates conditions of small scale reformers.

In view of these considerations, structured reactors based on conductive matrices have been proposed in the literature as a valuable new reactor layout that could mitigate the intrinsic limitations of energy demanding/non-adiabatic processes [8]. In particular, two main

* Corresponding author.

E-mail address: enrico.tronconi@polimi.it (E. Tronconi).

<https://doi.org/10.1016/j.cej.2019.123494>

Received 5 September 2019; Received in revised form 11 November 2019; Accepted 12 November 2019

Available online 13 November 2019

1385-8947/ © 2019 The Authors. Published by Elsevier B.V. This is an open access article under the CC BY-NC-ND license (<http://creativecommons.org/licenses/by-nc-nd/4.0/>).

Notation*Latin letters*

A	reactor outer surface [m ²]
Bi	Biot number = $h_w d_i / 2 / k_{eff}$ [-]
C _{eq}	overall internal conductance [W·m ⁻² ·K ⁻¹]
C _{p,mix}	heat capacity of outlet gas mixture [J·kg ⁻¹ ·K ⁻¹]
d	diameter [m]
F _{CH4} ⁱⁿ	methane inlet molar flow [mol·s ⁻¹]
H _{in}	enthalpy of the inlet flow [J·s ⁻¹]
H _{out}	enthalpy of the outlet flow [J·s ⁻¹]
h	heat transfer coefficient [W·m ⁻² ·K ⁻¹]
k	thermal conductivity [W·m ⁻¹ ·K ⁻¹]
L	length of the catalytic bed [m]
Q	thermal duty [W]
Re	Reynolds number = $\rho_g \cdot v \cdot d_p / \mu_g$ [-]
R	heat transfer resistance [W ⁻¹ ·m ² ·K]
Pr	Prandtl number = $\mu_g \cdot c_{p,mix} / k_g$ [-]
S _{v,F}	foam specific surface per unit volume [m ⁻¹]
U _{F→PB}	overall heat transfer coefficient for the packing material inside the foam matrix [W·m ⁻² ·K ⁻¹]
U _{overall}	global heat transfer coefficient [W·m ⁻² ·K ⁻¹]
v	gas velocity [m·s ⁻¹]
V _{react}	reactor volume [m ³]
W _p	mass of catalytic particles [kg]

Greek letters

δ _{gap}	effective heat transfer distance [m]
ε	void fraction [-]
μ	kinematic viscosity [Pa·s]
ρ	density [kg·m ⁻³]
ΔT	temperature difference [K]

Superscripts and subscripts

1–2	inlet section
3–4	outlet section
bed	catalytic section
cell	foam cell
eff	effective
eq	equivalentoverall
F	foam
g	gas
int	inside foam cells
p	catalytic particles
PB	packed bed
PF	packed foam
s	bulk foam material
strut	foam strut
t	tube
tot	total
w	wall

approaches can be followed to intensify the MSR process, namely the adoption of micro-flow reactors and the use of highly conductive internals.

In the first case, the steam reforming reaction is coupled with exothermic reactions in a multi-flow system, where FeCrAl-based reactors are used to run the process [9,10]. In such systems, the use of catalyst based on noble metals has been investigated, aiming at providing remarkable benefits with respect to conventional Ni-based catalysts, such as higher specific activity, faster dynamic response and better thermal and start/stop stability [11].

As an alternative, the adoption of thermally conductive metallic internals has been proposed to enhance heat transfer in fixed bed reactors with respect to conventional packed beds [8,12]. These metallic structures are available in various shapes (i.e. honeycomb monoliths, open cell foams) and they are usually made catalytically active by washcoating a thin layer of catalytic material onto their surface [13].

In view of the promising improvements that could be achieved by the use of conductive matrices, efforts have been reported in literature to investigate metallic supports for reforming applications. From the materials point of view, some constraints are present, as the steam reforming process is usually run at high temperature; thus, the bulk material of the structured supports has to be carefully chosen in order to match process specifications both from the physical and chemical point of view.

Many research groups have focused their attention on the use of steel-based materials, thanks to their good resistance to high temperature and chemical inertness in process conditions. Sang et al. used porous metallic 316 stainless steel foams as support for the production of a catalytic solar absorber based on Ni and Ru/Al₂O₃ catalysts for the CO₂ reforming of methane [14]. Yu et al. compared different materials (i.e. Ni, FeCrAl, Cu and CuZn alloy) as valuable bulk materials for high porosity open cell foams to be used as geometrical carriers of Cu-based catalysts for methanol steam reforming [15]. They demonstrated that the bulk material of metal foams plays an important role in the determination of overall process performance. Roy et al. published works aiming to optimize catalyst formulation and washcoat deposition for

the intensification of steam biogas reforming, using steel-based open cell foams [16,17].

Aluminum has been proposed in the literature as bulk material for structured supports but, due to its relatively low melting point (approx. 660 °C), it is suitable only for processes that are run at lower temperature than methane steam reforming, such as methanol steam reforming [18] and the Water Gas Shift process [19].

In some works, nickel and nickel-alloys open cell foams have been investigated as valuable supports for reforming process intensification. Park et al. proposed a hybrid technique of sol-gel and slurry methods to optimize the washcoating process onto nickel foams for the steam CO₂ reforming of CH₄ [20,21]. As a result of the heat transfer characteristics, the radial heat transfer of the metallic foam catalyst was improved with respect to catalytic alumina pellets.

Yang et al. investigated the use of nickel and copper open cell foams activated with Pd/Al₂O₃ for the combustion of methane, providing insights both on the washcoat deposition process and on the role of Ni and Cu metal foams on overall process performance [22].

On the other hand, copper has not been largely investigated as a valuable support, despite its relevant properties in terms of thermal conductivity and high temperature resistance. Moreover, most efforts have been spent in investigating copper supports for the intensification of methanol reforming: improved reactor performances were reported both by Zhou and co-authors [23] and by Shen et al. [24], who tested Cu/Zn/Al₂O₃/ZrO₂ catalysts and rare earth-promoted Cu-based materials, respectively. In particular, in the latter case, remarkable benefits in terms of heat transfer were reported, as a decrease of cold spot intensity was observed in copper supported systems over the packed bed configuration. Additionally, Catillon et al. demonstrated the beneficial influence of the introduction of copper structured matrices, which were activated by using a commercial Cu-ZnO/Al₂O₃ catalyst; in particular, improvements with respect to a commercial catalysts in form of pellets were reported [25].

As an alternative to methanol reforming, copper foams were tested in the solar dry reforming of methane by Qi et al., who carried out an experimental investigation of the catalytic activation of copper foams

using a Ni-based catalyst supported on Mg/Al oxides [26]. Copper-based supports were also investigated by Jang et al.: methane reforming and water splitting were tested using different types of washcoated foam devices under simulated solar-light irradiation, for the production of syngas and hydrogen [27].

Despite the high potential of washcoated structured supports, some drawbacks affect structured catalysts in comparison to the traditional packed bed configurations. In particular, the adoption of washcoated structures has intrinsic limitations in terms of catalyst inventory, which is usually smaller than in packed bed systems. In the case of processes limited by internal mass transfer (e.g. methane steam reforming) the catalyst load is in tradeoff with the effectiveness factor. Egg-shell pellets are typically employed in packed bed reactors to maximize the activity at fixed active species content, enabling a tuning of the thickness of the active layer. On the contrary, in the case of washcoated systems, for a given catalyst load, the thickness of the layer is a function of the geometric surface area of the support (i.e. $S_{v,F}$). To minimize the thickness, foams with high pore density (PPI = Pores per Inch) should be employed, whose activation by washcoating is however complex. Additionally, issues related to washcoat adhesion and catalyst loading/unloading have discouraged the application of this technology at the industrial scale [28].

In order to overcome such limitations, a new reactor configuration was recently proposed, which consists in filling the empty porosity of open-cell foams with small catalytic particles; the overall heat transfer properties of the system are enhanced by the highly conductive and interconnected matrices [28]. Accordingly, efficient removal of reaction heat is achieved also at low flow velocity, which allows to design short tubes reactors. Considering that: i) at fixed GHSV, pressure drops scale down with the 2nd to the 3rd power of the tube length; ii) in the same operating conditions the pressure drops of the packed foam reactor are only 5–10% higher than in a packed bed reactor of the same length and with the same particles, due to small changes in the total wetted surface area and in the void fraction [29] the adoption of short tubes enables the use of small catalytic pellets without detrimental effects on the compression duty. The concept of packed foams was first effectively applied to the strongly exothermic Fischer-Tropsch synthesis; the introduction of a highly conductive aluminum foam prevented the occurrence of thermal runaway, thus enabling to run the test reactor at much more severe conditions than in the packed bed configuration [30].

In a previous communication, the authors have reported the first application of copper-based matrices to the intensification of methane steam reforming, with very promising results. In particular, the adoption of copper-based layouts (i.e. packed foams and washcoated foams) resulted in a global improvement of system performance over the conventional packed bed configuration [31]. Based on those results, in this work an experimental investigation is carried out to further explore how the introduction of conductive matrices may improve the overall MSR reactor performance. Accordingly, different reactor configurations were tested and compared, namely a FeCrAl packed foam and two copper packed foam systems with different cell densities. A traditional packed bed system was also tested, as benchmark of traditional layout for the reforming process. In all cases, the same Rh/Al₂O₃ catalyst in

form of egg-shell particles with 600 μm diameter was used. Finally, a predictive heat transfer model of the packed foams was developed, based on the approach of electric equivalent circuit and incorporating independently estimated effective parameters: the model was validated against the experimental results and used to analyze and interpret the observed effects. The herein collected evidence paves the way to future optimization of the methane steam reforming reactor aiming at the maximization of the productivity or at an optimal tradeoff between fixed and operational costs [32].

2. Experimental

2.1. Catalyst preparation and characterization

Catalytic tests were performed using a home-made Rh/Al₂O₃ catalyst in the form of egg-shell particles. The procedure, reported by Porta et al. [33], is herein briefly summarized. Alumina particles (Puralox by Sasol, 600 μm nominal diameter) were preliminary dried in a static oven at 120 °C overnight; then, Rh was deposited by incipient wetness impregnation. A Rh(NO₃)₃ liquid solution (12.5 %wt metal content by Alfa Aesar) was diluted with deionized water, aiming both to fill alumina porous volume and to meet the final rhodium content. Dilution water was calculated according to the material pore volume (i.e. 0.47 ml·g⁻¹); based on results reported in literature, an additional quantity of water equal to the 25% of pore volume was added to better manage eggshell morphology and homogeneity [33]. The final Rh metal content was set to 0.3 %wt with respect to alumina carrier mass. After impregnation, particles were dried overnight at 120 °C.

As received alumina particles and catalytically activated alumina were characterized in terms of specific surface area and porosity by liquid nitrogen adsorption/desorption isotherms at -196 °C on Micromeritics ASAP 2020 instrument; properties were calculated according to the Brunauer-Emmet-Teller (BET) equation. A specific surface area of 160 m²·g⁻¹ was found for the bare Al₂O₃ particles.

Effective catalyst composition was measured by ICP-MS analysis using an X Series II instrument by Thermo Fischer.

Temperature programmed reduction and pulse techniques were applied to evaluate the Rh dispersion. Tests were performed using a TPD/R/O 1100 catalytic surface analyzer by Thermo Electron. Metal dispersion was calculated as the ratio between the number of surface metal atoms and the total number of metal atoms of the sample [34]. A summary of the operating conditions used for samples characterization is reported in Table 1. Metal dispersions in the range of 90% were found for the fresh egg-shell catalyst.

A scanning electron microscope (ZeissEvo50 EP) equipped with an energy dispersive X-ray spectrometer (EDX, Oxford Inca Energy 200 - Pentafet LZ4) was used to determine the concentration profile of rhodium in the radial direction of sectioned catalytic pellets.

Foam cell diameter and strut shape were evaluated by means of optical microscopy. The total porosity was estimated by gravimetric analysis from the foam volume, mass and bulk metal density. The hydraulic porosity was measured by ethanol picnometry, as reported in literature [35]. Negligible differences between the total and the hydraulic porosities were observed. Thus, only the hydraulic porosity (ϵ_F)

Table 1

Summary of operating conditions for the chemisorption measurements: 10 pulses with sampling loop volume equal to 0.961 cm³.

Step no.	Step description	Temperature	Heating ramp	Hold time	flow rate [cm ³ ·min ⁻¹ NTP]	Flow composition
1	Heating	R.T. → 150 °C	10 °C/min	30'	50	He
2	Reduction	150 °C → 500 °C	10 °C/min	1 h	50	H ₂
3	Purge	500 °C	–	1 h	50	He
4	Cooling	500 °C → R.T.	–	–	50	He
5	Pulse	R.T.	–	–	30	5% H ₂ in Ar

Catalyst pellet diameter and egg-shell thickness were evaluated by means of optical microscopy, using a SterEO Discovery.V12 instrument equipped with an Axiocam ERc 5 s camera by Zeiss.

will be reported in the characterization section, in Table 2.

2.2. Catalytic tests

Experiments in the packed foam configuration were performed using different materials for the open cell internals. In the case of the steel-based supports, FeCrAlY open cell foams (Porvair) of 12 PPI with 5.2 mm cell size and 0.92 void fraction (ϵ_F) were used (FeCr12 in the following). In the case of copper-based open cell foams, two different samples were tested, with 10 PPI and 40 PPI nominal porosities, respectively (Cu10 and Cu40). In the former case, the cell size was equal to 4.6 mm ($\epsilon_F = 0.91$), while in the latter case the cell size was equal to 2 mm ($\epsilon_F = 0.88$). For all the tested structures, diameter and height of the foam samples were set at 29 mm and 25 mm, respectively. Table 2 reports the main open cell foams properties. In addition to the tests with the packed foam configuration, tests in a conventional packed bed system (no foam) were also run. In this configuration, the same mass of catalytic particles per unit volume was loaded in the reactor. In order to ensure the same reactor volume, the catalyst bed was diluted with inert SiC particles (SiC to catalyst weight ratio = 1.54).

Graphical representations of the top-view of the reactor cross section are shown in Fig. 1.

In all configurations, catalytic tests were performed in a tubular reactor with an internal diameter of 29.5 mm: Fig. 1c shows a graphical representation of the reactor longitudinal section. Using a bottom-up approach, an empty and inert FeCrAl foam is put in straight contact with a soldered plate, which is located in the middle of the reactor. A thin layer of FeCrAl felt is inserted in the reactor to hold the catalytic bed in the proper position. Then, the catalytic bed is loaded, either in packed bed or packed foam configuration. In the latter case, first the metallic foam is inserted into the reactor; then, catalyst particles are poured to fill the foam cavities. In order to improve the packing efficiency, the reactor is gently shaken during the catalyst loading process.

In order to allow reactant mixing, the upper part of the reactor was filled with inert silicon carbide particles. A thin steel wire mesh was inserted between the catalytic bed and the silicon carbide bed, in order to prevent mixing of the catalyst with the inert material in the reactor loading process.

Catalytic tests were performed at two different space velocities, namely 5000 and 10,000 h^{-1} . Flow rates were calculated referring to the equivalent volume of a pure packed bed system. In all reactor configurations, the same mass weight of catalyst (namely 5.75 g) was

loaded and the same catalytic bed volume was used for all the experiments. The reactor was heated externally by a furnace (RT 50/250/11 model by Nabertherm) and catalytic tests were performed in the 600–800 °C range, with 50 °C steps, at atmospheric pressure.

The reactants feed consisted of a steam/ CH_4 mixture with S/C ratio of 3.5. Methane was fed with an EL-FLOW flow regulator/controller (model F-201CV by Bronkhorst), while water was fed in liquid form using a Bronkhorst flow regulator/controller (Cori-flow model M12V14I). Reactants were fed independently to the reactor; the evaporation and reactant mixing took place in the SiC premixing bed.

In order to measure axial temperature profiles across the catalytic bed, holes were drilled for the thermocouple-wells both in the packed foams and in the foam downstream the catalytic bed. In particular, three different radial positions were chosen, namely at the centerline (CT in the following), at 8 mm from the center in radial direction (RT) and at the outer reactor wall (WT), as sketched in Fig. 1a and c. Temperature was measured with a resolution of 5 mm, on a total length of 7.5 cm. The foam void volumes were filled with catalytic particles, as reported in Fig. 1b, where the Cu40 foam is shown during the packing process. Temperature profiles were recorded both in reactive and non-reactive conditions. In the latter case, catalytic pellets were replaced with an equal mass of inert alumina pellets in order to perform tests at the same flow rate, feed composition and GHSV.

At the reactor outlet, unreacted water was condensed and separated downstream from the reactor. A nitrogen flow was mixed to the dry product stream, using a flow regulator/controller by Brooks instruments (SLA5850 model) and was used as internal standard for the gas analysis.

The quantification of reaction products was performed using an online micro-GC (GCX model by Pollution) equipped with MolSieve and Porapak columns connected to TCD detectors. Water was calculated according to methane consumption and CO_2 production. The overall absolute errors detected in carbon balances were in the range of 1–5%.

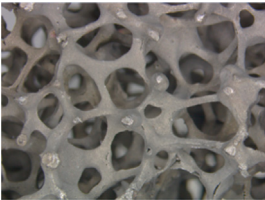
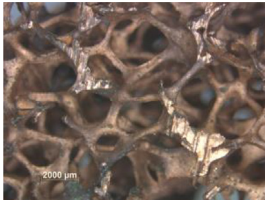
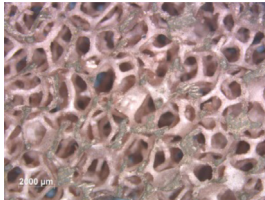
3. Results and discussion

3.1. Catalyst characterization

The catalytic material was characterized according to the procedures reported in Section 2.1. The total metal content, in terms of Rh^0 with respect to the Al_2O_3 matrix, was found to be equal to 0.28 %wt, which is in good accordance with the specification (0.3 %wt). Eggshell

Table 2

Geometrical properties of open cell foams. In all cases, foam height and diameter are equal to 25 mm and 29 mm, respectively. *Dilution ratio is calculated as the weight ratio between dilutant mass and catalyst mass. $S_{V,F}$ and d_{strut} were calculated according to [39]. **Catalyst inventory is calculated as the ratio between catalyst pellet mass and catalytic section volume.

	FeCr12	Cu10	Cu40
			
PPI	12	10	40
ϵ_F [-]	0.92	0.91	0.88
$S_{V,F}$ [m^{-1}]	500	600	1220
d_{cell} [mm]	5.2	4.6	2
d_{strut} [μm]	745	705	285
Strut shape	Triangular	Triangular	Circular
Dilution material	Al_2O_3	Al_2O_3	Al_2O_3
ϵ_{PF}	0.4	0.4	0.42
Dilution ratio*	0.63	0.58	0.51
Catalyst inventory [$\text{kg}\cdot\text{m}^{-3}$]**	348	348	348

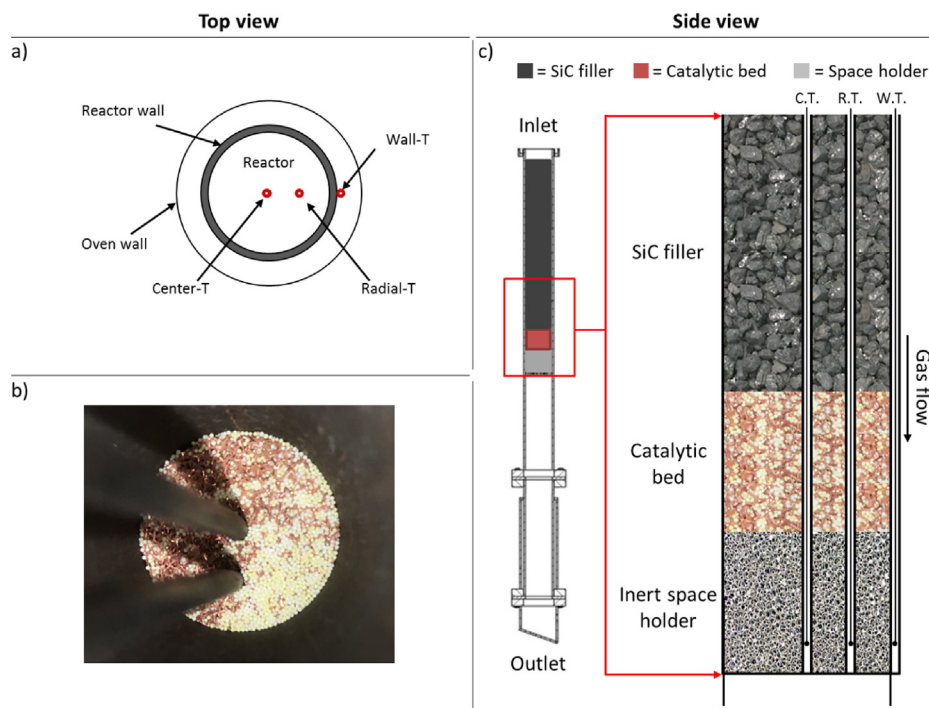


Fig. 1. Top view graphical representation of the reactor layout (a), top view of a Cu40 foam loaded into the reactor during packing procedure (b) and graphical representation of the reactor layout, side view (c).

thickness was evaluated by cross section analysis, whose results are reported in Fig. 2.

The thickness of the egg-shell layer was found to be $38 \pm 2 \mu\text{m}$ (Fig. 2a), which is consistent with results reported in literature for catalysts produced with a similar preparation procedure [33]. The SEM-EDX characterization reported in Fig. 2b confirmed the thickness of the egg-shell layer, pointing out a linear increase of Rh content in the outer shell of the catalyst particle.

It is worth noting that a $40 \mu\text{m}$ shell thickness corresponds well to recommendations of catalyst manufacturers [36] to avoid overuse of costly active phases in the presence of severe internal mass transfer limitations associated with the very fast steam reforming kinetics at high temperature. Preliminary calculations based on the rate equations proposed by Donazzi et al. [37] for a Rh/Al₂O₃ system show that significant limitations arise with a shell thickness of more than $40 \mu\text{m}$ at 700°C . Despite of this severe limit on the shell thickness, the use of 0.6 mm spheres (surface to volume ratio of about 5000 m^{-1}) results in a catalyst inventory that widely exceeds the one of washcoated 40 PPI foams with the same Rh concentration and coating thickness; in fact, in

the case of washcoated foams the same load can be reached only using supports with extremely high pore density (100 PPI), which poses however severe challenges to the coating process.

In order to have a preliminary evaluation of the catalytic performance of the home-made catalyst, tests at high space velocity ($25,000 \text{ NL-kgcat}^{-1}\text{-h}^{-1}$) were performed in a small-scale lab rig with diluted feed (CH₄ concentration of 1%, S/C ratio equal to 3.5, N₂ complement), according to the procedure reported in [38]. In these operating conditions, the measured conversion of CH₄ at high temperature was close to the thermodynamic equilibrium, which confirmed that a suitably active formulation was obtained, enabling its further use in concentrated feed conditions.

3.2. Catalytic tests

As above mentioned, four different reactor configurations were tested, namely a packed bed, a 12 PPI FeCrAl packed foam (FeCr12 PF), a 10 PPI copper foam (Cu10 PF) and a 40 PPI copper packed foam (Cu40 PF). Due to the differences in reactor layout, variable dilutions

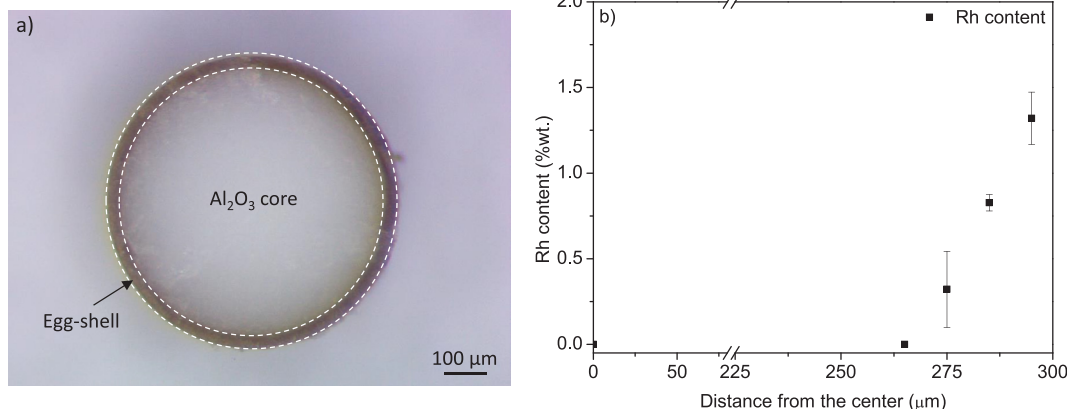


Fig. 2. Cross section analysis of a $600 \mu\text{m}$ egg-shell catalytic particle (a) and results of SEM-EDX analysis of Rh concentration profile across particle section (b).

were needed in order to ensure the same mass of catalyst per unit reactor volume. A summary of catalytic bed dilution conditions is given in Table 2, together with the morphological parameters of the tested foams.

Foam surface area ($S_{V,F}$) and strut diameter (d_{strut}) were calculated according to the model of Ambrosetti et al., using d_{cell} , ε and strut shape as input parameters [39]. A small variation in the packing density inside the cavities was observed, due to the different cell sizes and porosities of the foams. A traditional packed bed configuration (labelled as "PB" in the following) with the same catalyst load was also tested as a reference; in this case, the bed was diluted with SiC pellets with a dilution ratio equal to 1.54 (SiC/catalyst weight ratio).

In Fig. 3, the temperature profiles measured in the four reactor layouts are plotted against the distance from the bottom of the reactor.

Results refer to the tests performed at GHSV $10,000 \text{ h}^{-1}$; for the sake of simplicity, only results obtained for the furnace temperature set at $800 \text{ }^\circ\text{C}$ were plotted. Full symbols refer to temperature profiles measured in reacting conditions, while empty symbols correspond to the temperature profiles measured in inert flow conditions; in the latter blank tests, no catalytic activity was detected.

The strong endothermic behavior associated with the steam reforming process is evident in all the temperature profiles, as a remarkable negative temperature difference is present between the center and the wall of the reactor. Apparently, the introduction of the FeCrAl foam (Fig. 3b) into the catalytic bed did not bring any clear improvement to the temperature profile over the packed bed configuration (Fig. 3a): the maximum radial temperature drop from the wall was similar in the two configurations ($132 \text{ }^\circ\text{C}$ for FeCr12 and $120 \text{ }^\circ\text{C}$ for PB system, respectively) and the internal temperature gradients were also similar (i.e. the difference in the cold-spot between the measurement at the centerline and the radial measurement at $r = 8 \text{ mm}$).

The adoption of copper foams provides instead remarkable benefits. A significant change is apparent in the relative distance between the central and radial temperature profiles, which are significantly different in the packed bed and in the packed FeCr12 system (Fig. 3a, b, full square and full circle lines), while they almost overlap in the copper systems (Fig. 3c and d). This behavior can be ascribed to the higher conductivity of copper ($380 \text{ W}\cdot\text{m}^{-1}\cdot\text{K}^{-1}$) with respect to FeCrAlloy ($16 \text{ W}\cdot\text{m}^{-1}\cdot\text{K}^{-1}$), which results in a more efficient radial and axial heat transfer and allows for a more uniform temperature distribution across

the catalytic bed. A further improvement is observed moving from the configuration c) (i.e. 10 PPI copper packed foam) to the configuration d) (i.e. 40 PPI copper packed foam), where the distance between the wall temperature and the internal profile is reduced, most likely due to an improvement of the wall heat transfer coefficient.

The heat transfer properties of the system, which are characteristic of each configuration, apparently affect also the position where the maximum temperature drop is located. Moving from Fig. 3a–d, the cold spot is progressively shifted towards the catalytic bed inlet. This is probably due to the superposition of different phenomena. When a configuration with inferior heat transfer capabilities is tested (e.g. PB or FeCrPF), more pronounced temperature gradients are manifest. Thus, due to the lower temperature (i.e. slower kinetics), the equilibrium conversion is reached at a greater distance from the inlet, which directly translates into a shift of the temperature drop towards the end of the catalytic bed. In the Cu based systems, instead, the heat requirement of the process is readily fulfilled and, thus, less pronounced peaks are observed already closer to the catalytic bed inlet. Similar results were obtained at other GHSV and oven temperatures.

In order to gain a more comprehensive view of the performance of the different layouts, the maximum radial temperature difference across the catalytic bed was plotted as a function of the oven temperature (Fig. 4).

The points at $800 \text{ }^\circ\text{C}$ correspond to the maximum radial temperature difference between the full star and the full square lines reported in panels a, b c and d of Fig. 3. As introduced before, according to these results the presence of the FeCrAl matrix apparently does not bring about any benefit in comparison with the packed bed system; on the opposite, the thermal behavior is apparently even worse. This can be explained by the beneficial effect of the conductive diluent (SiC particles) in the present packed bed configuration, which may play a significant role in improving the heat transfer properties of the packed bed system at low Reynolds numbers. By this practice, the static thermal conductivity of the bed is slightly increased.

At any furnace temperature, on the other hand, results are significantly different when highly conductive internals are adopted: by changing the bulk material of open cell foams from FeCrAl to copper (i.e. from $16 \text{ W}\cdot\text{m}^{-1}\cdot\text{K}^{-1}$ to $380 \text{ W}\cdot\text{m}^{-1}\cdot\text{K}^{-1}$ in terms of bulk thermal conductivity) a remarkable change of the heat transfer performance of the system is noted. At the highest furnace temperature, the maximum

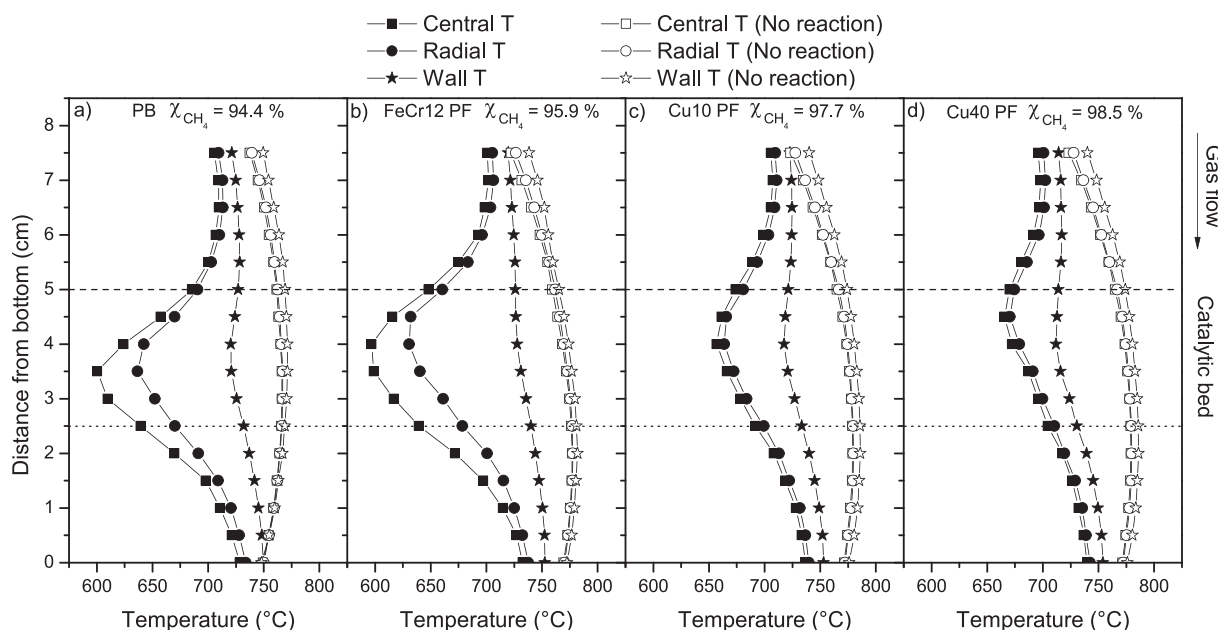


Fig. 3. Axial temperature profiles measured at three radial positions at $800 \text{ }^\circ\text{C}$ and GHSV = $10,000 \text{ h}^{-1}$. Full symbols refer to reaction conditions, empty symbols correspond to inert conditions. Dashed line and dotted line indicate catalytic bed inlet and outlet, respectively.

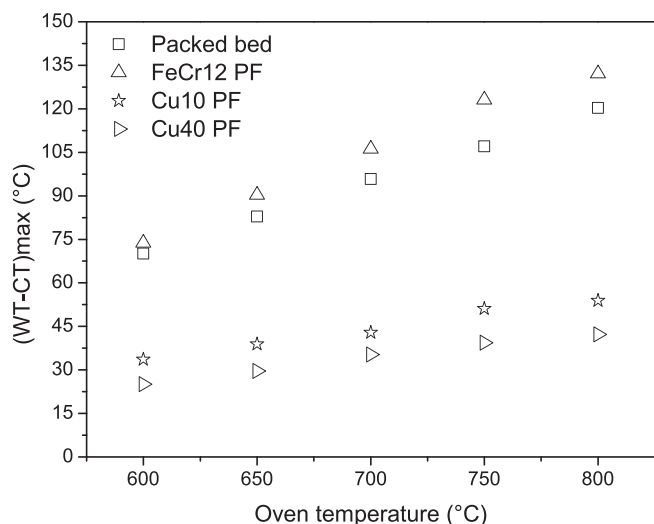


Fig. 4. Maximum radial temperature difference between wall thermocouple (WT) and central thermocouple (CT), as a function of furnace temperature. GHSV equal to $10,000 \text{ h}^{-1}$.

radial temperature difference drops from $132 \text{ }^\circ\text{C}$ (for the FeCr12 packed foam configuration) to $40 \text{ }^\circ\text{C}$ (for the Cu40 packed foam layout). Similarly, important drops of the radial temperature gradients occurred under all the tested conditions.

In addition to the characterization of the temperature profiles, Fig. 5 shows the conversions of methane at increasing measured outlet temperature and oven temperature.

Fig. 5a compares the methane conversion and the equilibrium conversion as a function of outlet temperature at $r/2$; the latter was assumed as a representative reference temperature for the calculation of the equilibrium conversion, given the good accordance between the experimental and the computed equilibrium composition data at high temperature, where the system works at thermodynamic equilibrium. For all the supports, at bed temperatures below $650 \text{ }^\circ\text{C}$ the conversion is lower than that at equilibrium, therefore kinetic limitations are present, whereas, independently from the foam material, the measured conversion is almost superimposed to the calculated equilibrium curve at T greater than $650 \text{ }^\circ\text{C}$, thus excluding artifacts associated with the presence of a structured metallic internal in the reactor. In particular, the metallic insert does not prevent achieving high reaction rates and high conversions, which rules out possible negative interactions with the catalytic formulation (e.g. poisoning effects).

Remarkable improvements of methane conversion of the packed

foam configuration over the packed bed layout become manifest instead when data are compared at fixed furnace temperature (Fig. 5b). In this plot, the continuous line represents the thermodynamic equilibrium calculated at oven temperature, which corresponds to the process limit of the system. The increase in methane conversion is especially relevant when copper matrices are present. As an example, at an oven temperature of $700 \text{ }^\circ\text{C}$, conversion shifts from 75.3% in packed bed configuration to a maximum of 86.4% , which is reached with the 40PPI copper foam. The improved methane conversion is ascribed to the flattening of the temperature profiles inside the whole catalytic bed, due to the adoption of the conductive Cu internals. As a result, the reactor operates at higher catalyst temperatures, thus with improved reaction kinetics, throughout the bed. Thermal efficiency and H_2 efficiency of the new reactor design are thus both improved, being strictly interconnected performance indicators.

At higher oven temperatures the system approaches chemical equilibrium and the increase in the conversion is limited. Notice however that the advantage may be more substantial at higher space velocities.

3.3. Assessment of process thermal duty

An overall analysis of the different reactor layouts can be obtained by evaluating the thermal duty associated with the steam reforming process in the experiments (Q_{bed} , W). Fig. 6 shows a schematic representation of the test reactor configuration and of the associated temperature profiles. By looking at the temperature profiles, it is evident that the temperatures upstream and downstream the catalytic bed are influenced by the reaction, with the onset of axial heat transfer between the different zones of the reactor. Some considerations are therefore required to exclude from our analysis the impact of the thermal back-conduction on the estimates of the overall heat transfer coefficient. The boundaries of our system were set where almost null temperature gradients are present in the profiles. Accordingly, we can divide this new system in three zones, where three different packings are present. In the first zone (1–2) a packed bed of SiC particles is present, in the second zone (2–3) the four different reactor layouts of the study are loaded and in the third zone (3–4) an inert FeCrAlloy foam is loaded.

Based on the representation of Fig. 6, the total thermal duty (Q_{tot}) can be calculated as Eq. (1)

$$Q_{\text{tot}} = H_{\text{out}} - H_{\text{in}} \quad (1)$$

Where H_{in} is the enthalpy of the reactants (boundary 1, Fig. 6) at the inlet and H_{out} is the enthalpy of the product stream, at the outlet (boundary 4, Fig. 6). In the present configuration, the reaction takes

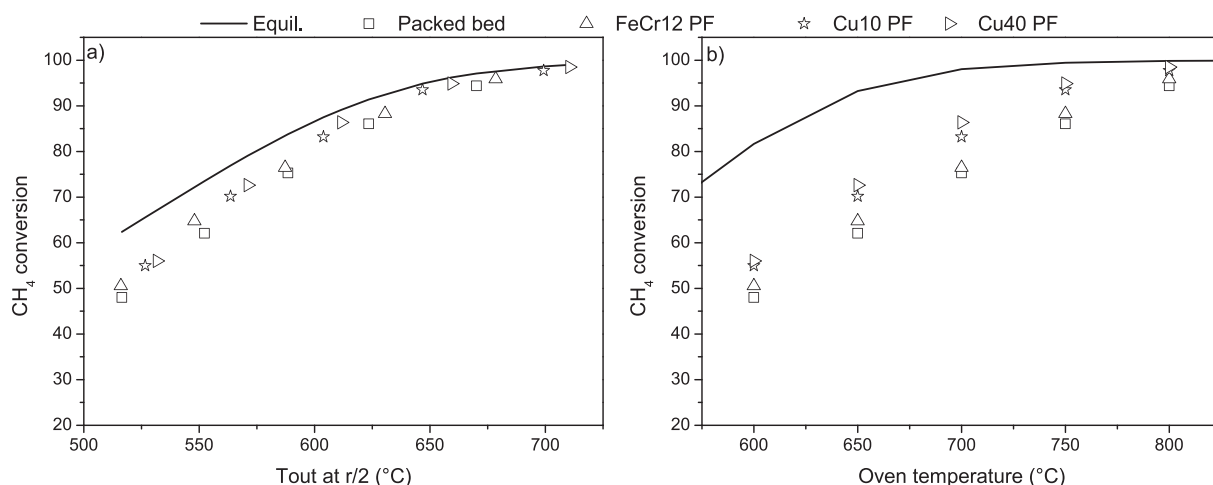


Fig. 5. Methane conversion as a function of outlet temperature in radial position (a) and of oven temperature (b).

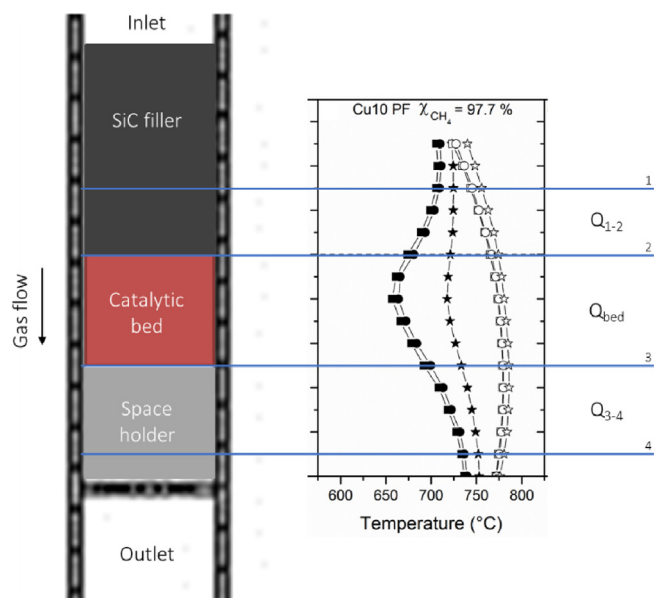


Fig. 6. Schematic representation of the system boundaries.

place in the catalytic bed, where, accordingly, the cold-spot of the configuration is located. The heat for the reaction may be supplied by all the three zones, therefore the total thermal duty can be divided in three different contributions - Eq. (2)

$$Q_{tot} = Q_{1-2} + Q_{bed} + Q_{3-4} \quad (2)$$

where Q_{1-2} (W) is the thermal duty of the inlet section, Q_{bed} (W) is the thermal duty associated with the reforming process in the catalytic bed and Q_{3-4} (W) is the thermal duty of the outlet section.

The thermal duties of the inlet and outlet section can be calculated according to correlations reported in literature. As far as Q_{1-2} is concerned, the parameter refers to a reactor section composed by a packing of inert SiC particles (d_p of 4 mm). The expression for Q_{1-2} is reported in Eq. (3)

$$Q_{1-2} = \frac{U_{1-2} \cdot A \cdot \int_1^2 \Delta T(x) dx}{L} \quad (3)$$

Where U_{1-2} ($\text{W}\cdot\text{m}^{-2}\cdot\text{K}^{-1}$) is the overall heat transfer coefficient in the upstream section, A (m^2) is the cylindrical exchange area of the reactor, ΔT (K) is the difference between the temperature of the external wall thermocouple (WT) and the radial thermocouple (RT) along the axial coordinate and L (m) is the section length. U_{1-2} was calculated according to correlations by Specchia et al. [40]; a detailed description is reported in the S.2 of the Supplementary material.

Using a similar approach, the thermal duty of the outlet section (Q_{3-4} , W) can be calculated according to Eq. (4);

$$Q_{3-4} = \frac{U_{3-4} \cdot A \cdot \int_3^4 \Delta T(x) dx}{L} \quad (4)$$

where U_{3-4} ($\text{W}\cdot\text{m}^{-2}\cdot\text{K}^{-1}$) is the overall heat transfer coefficient in the outlet section. This section includes an empty FeCrAl open cell foam (ϵ_F and d_{cell} equal to 0.91 and 2 mm, respectively). U_{3-4} was estimated according to Aghaei et al. [41]; the calculation is fully detailed in S.2.

Eventually, Q_{bed} is calculated by difference according to Eq. (2); results are shown in Fig. 7 as a function of the difference between the temperature of the external wall thermocouple (WT) and the radial thermocouple (RT) averaged over the catalytic bed along the axial coordinate (x).

When Q_{bed} is plotted as a function of the average radial temperature difference (Fig. 7) in the catalytic bed zone, a preliminary evaluation of

the overall heat exchange performance of each reactor configuration can be obtained from the slope of the corresponding trend lines. The packed bed and the FeCr12 PF systems display similar trends (namely similar moderate slopes of the plots), such that increasing heat flows (and H_2 productivities) were obtained at the expense of increasingly important radial temperature gradients and thus loss of efficiency in the catalyst utilization. Increased slopes, corresponding to improved heat transfer, are manifest in the copper-based systems, where larger productivities were measured with smaller average temperatures of the catalytic bed. The best overall heat transfer performances are clearly achieved by the Cu40 PF system.

3.4. Estimate of global heat transfer coefficient in the catalytic bed

More accurate evaluations of the heat transfer performance were performed for each reactor configurations under the single operating conditions herein explored; at this scope, the global heat transfer coefficient ($U_{overall}$, $\text{W}\cdot\text{m}^{-2}\cdot\text{K}^{-1}$) was calculated according to Eq. (5) and plotted in Fig. 8 as a function of the oven temperature, taken as an independent descriptor of the changing thermal and reaction conditions of the system.

$$U_{overall} = \frac{Q_{bed} \cdot L}{A \cdot \int_2^3 \Delta T(x) dx} \quad (5)$$

The integral of ΔT (K) as a function of x is the average difference between the temperature of the external wall thermocouple (WT) and the radial thermocouple (RT) over the catalytic bed along the axial direction (x).

Packed bed and FeCr PF systems show similar values of $U_{overall}$, ranging from 200 to 300 $\text{W}\cdot\text{m}^{-2}\cdot\text{K}^{-1}$, depending on temperature and reaction conditions. A remarkable increase of $U_{overall}$ is estimated when copper matrices are used, as the overall coefficient is two to three times higher than in the PB system, reaching values in the range of 450 and 750 $\text{W}\cdot\text{m}^{-2}\cdot\text{K}^{-1}$ for Cu10 PF and Cu40 PF, respectively. This clearly emphasizes the beneficial contribution of the conductive matrices to the overall heat exchange performance at these reaction conditions. A more marked dependence of the coefficient $U_{overall}$ on the reaction regime, changing with increasing oven temperature, is also apparent.

3.5. Heat transfer model-based analysis

Following the approach described in [28], radial heat transfer in packed foams is described according to an electric-equivalent circuit as

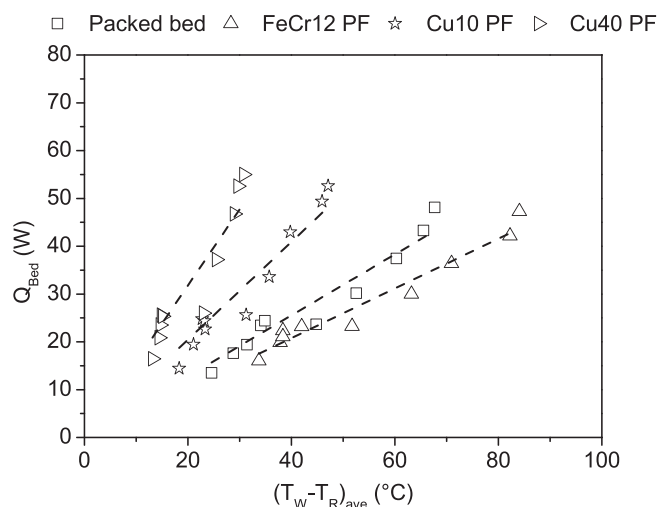


Fig. 7. Thermal duty of MSR as a function of the radial average temperature difference in the middle of the catalytic bed.

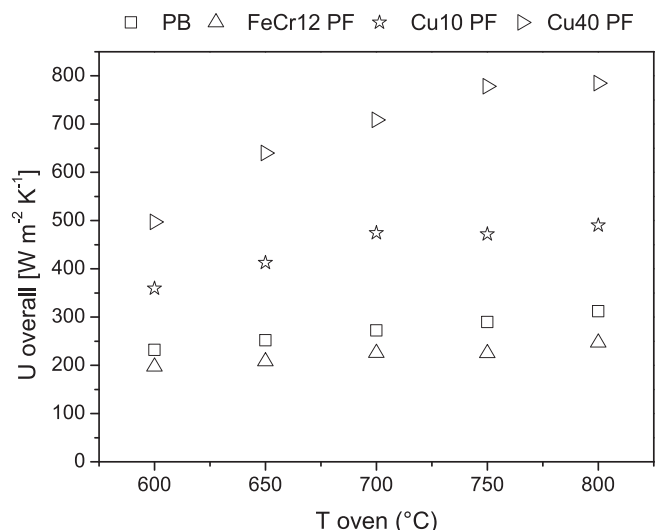


Fig. 8. Overall heat transfer coefficient as a function of oven temperature.

shown in Fig. 9. Two parallel heat flow paths are considered: one associated with the foam interconnected structure ($k_{\text{eff},F}$ = effective radial thermal conductivity of the foam); the other associated with the fluid phase and the packed particles, which are lumped together in a single pseudo phase according to the heat transfer literature for packed beds [39] ($k_{\text{eff},PB}$ = effective radial thermal conductivity of packed bed). Following classical literature approaches, a separated near wall resistance is considered for both the foam ($h_{w,F}$ = wall heat transfer coefficient of foam structures) and the lumped fluid phase-packed particle systems ($h_{w,PB}$ = wall heat transfer coefficient in packed beds). The near-wall resistances are combined in parallel assuming that the two paths are short circuited before entering in the bed core. Differently from [28], all the elements in the circuit are considered in order to cover a more extensive range of materials, geometries and operating parameters. Besides, an additional term, $U_{F \rightarrow PB}$, is introduced in order to take into account the internal resistance associated with heat transfer from the foam struts to the packed bed, under the assumption that the T-measurements provided by the thermocouple are representative of the temperature of the lumped fluid-packed particles phase.

In this work, the radiative contribution was not considered, both for the packed bed and for the foam phase. In the first case, a sensitivity analysis based on the VDI Wärmeatlas [42] correlations revealed that radiation does not provide any significant contribution to the effective conductivity of the herein tested packed bed configurations. The same assumption was extended to the packed foam configurations in view of the close geometrical similarity with packed beds obtained by filling the empty foam cells with small catalyst (and inert) particles.

All the terms in the equivalent circuit of Fig. 9 have been derived from the literature and combined as in parallel-in-series resistances.

The scheme in Fig. 9 can be divided in two in-series blocks, the near-wall one and the internal one, accordingly the global heat transfer coefficient (U_{overall} , $\text{W}\cdot\text{m}^{-2}\cdot\text{K}^{-1}$) can be expressed as in Eq. (6)

$$U_{\text{overall}} = \left(\frac{1}{h_{w,eq}} + \frac{1}{C_{eq}} \right)^{-1} \quad (6)$$

where $h_{w,eq}$ is a lumped wall heat transfer coefficient resulting from the combination of the two parallel mechanisms at the wall, while C_{eq} is a cumulative conductance term that takes into account all the heat transfer terms across the core of the catalytic bed. In the following paragraphs, the two contributions will be described in detail.

3.5.1. Near-wall equivalent resistance

According to the in parallel arrangement, the overall wall heat transfer coefficient can be obtained as the sum of the packed bed and

the foam contribution:

$$h_{w,eq} = h_{w,PB} + h_{w,F} \quad (7)$$

In this work, $h_{w,PB}$ is calculated as reported in Eqs. (8)–(10) adopting the correlations for packed beds proposed by Specchia et al. [40].

$$h_{w,PB} = h_{w,PB,static} + h_{w,PB,convective} \quad (8)$$

$$h_{w,PB,static} = \left(\frac{k_g}{d_p} \right) \left(2\varepsilon_{PF} + \frac{1 - \varepsilon_{PF}}{0.0024} \cdot \left(\frac{d_t}{d_p} \right)^{1.58} + \frac{1}{3} \frac{k_g}{k_{s,p}} \right) \quad (9)$$

$$h_{w,PB,convective} = \left(\frac{k_g}{d_p} \right) 0.0835 \cdot Re^{0.91} \quad Re < 1200 \quad (10)$$

Re is the Reynolds number (referred to the particle diameter). The thermal conductivity of the solid particles was assumed equal to $1 \text{ W}\cdot\text{m}^{-1}\cdot\text{K}^{-1}$, while the thermal conductivity of the particles in the SiC-diluted packed bed was set equal to $2.41 \text{ W}\cdot\text{m}^{-1}\cdot\text{K}^{-1}$; this latter value was calculated according to equations reported in literature for the evaluation of the properties of mixed packed systems [43]. The gas thermal conductivity, as well as all other gas properties, were calculated based on the mixture composition and temperature at the catalytic bed outlet. A summary of the measured composition of outlet gas and of the calculated gas properties is presented in the Supplementary material (S.1).

ε_{PF} is the void fraction of the packing pattern in the foam cavities evaluated as:

$$\varepsilon_{PF} = \frac{V_{\text{react}} \varepsilon_F - W_p / \rho_p}{V_{\text{react}} \varepsilon_F} \quad (11)$$

The packing efficiency that was measured experimentally is reported in Table 2: it varies from 0.4 to 0.42 from 10 PPI to 40 PPI foams. These values are in agreement with the recent study of Ambrosetti et al. [29].

For the foam contribution only the static term of the wall heat transfer coefficient described in [41] has been considered, assuming that the flow pattern in the near-wall region is governed by the packed particles. The wall heat transfer coefficient is calculated dividing the gas thermal conductivity by the gap distance between foam and wall.

$$h_{w,F} = \frac{k_g}{\delta_{\text{gap}}} \quad (12)$$

δ_{gap} (m) represents an effective heat transfer distance and can be calculated according to (13) [41]:

$$\delta_{\text{gap}} = 0.00013 + 0.14 d_{\text{cell}} \quad (13)$$

3.5.2. Internal resistance

The overall internal conductance (C_{eq}) can be evaluated by considering an in-parallel resistance network:

$$C_{eq} = \left(\frac{R_{PB} R_F}{R_{PB} + R_F} \right)^{-1} \quad (14)$$

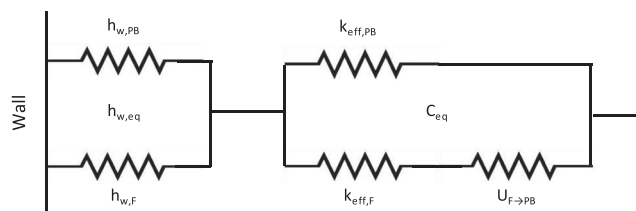


Fig. 9. Graphical representation of the heat transfer mechanisms within packed foams using an equivalent circuit of resistances.

In Eq. (14), R_{PB} describes the heat transfer resistance throughout the combined fluid and packed particles, treated as a single pseudo-phase: R_F refers to the path via the interconnected foam structure and also includes the interphase heat transfer from the foam struts to the catalyst particles. The expression for R_{PB} is derived from the classical packed bed literature [44]:

$$R_{PB} = \left(\frac{d_t}{6.13 \cdot k_{eff,PB}} \right) \quad (15)$$

In Eq. (15), $k_{eff,PB}$ ($W \cdot m^{-1} \cdot K^{-1}$) is the effective thermal conductivity of the packed bed and is evaluated according to Specchia et al. [40].

$$k_{eff,PB} = \left[k_g \cdot \varepsilon_{PF} + \frac{k_g(1 - \varepsilon_{PF})}{0.22 \cdot \varepsilon_{PF}^2 + \frac{2}{3} \frac{k_g}{k_{s,p}}} \right] + \left[k_g \frac{Re \cdot Pr}{Pe_{RIF}} \right] \quad (16)$$

Re and Pr are the Reynolds (referred to the particle diameter) and Prandtl numbers, respectively, while Pe_{RIF} is calculated according to Eq. (17) [40].

$$Pe_{RIF} = 8.65 \left(1 + 19.4 \left(\frac{d_p}{d_t} \right)^2 \right) \quad (17)$$

The lower branch of the thermal circuit, which corresponds to R_F , is composed by the series of the resistances to the heat flow in the solid phase and at the interface between the two phases. A general expression for R_F can be written as in Eq. (18), where the first term refers to the conduction in the solid matrix and the second term refers to the interfacial resistance.

$$R_F = \left(\frac{d_t}{6.13 k_{eff,F}} + \frac{4}{d_t S_{V,F} U_{F \rightarrow PB}} \right) \quad (18)$$

$k_{eff,F}$ ($W \cdot m^{-1} \cdot K^{-1}$) is the metallic foam effective conductivity and $U_{F \rightarrow PB}$ ($W \cdot m^{-2} \cdot K^{-1}$) is an overall heat transfer coefficient of a pseudo packed bed channel with a diameter equal to the cell size of the foam. $k_{eff,F}$ is estimated according to Braconci et al. [45],

$$k_{eff,F} = \left[\frac{1}{3} + \frac{2}{3}(1 - \varepsilon_F) \right] (1 - \varepsilon_F) k_{s,F} \quad (19)$$

where $k_{s,F}$ ($W \cdot m^{-1} \cdot K^{-1}$) is the solid bulk conductivity of the foam material, which was assumed equal to $16 W \cdot m^{-1} \cdot K^{-1}$ and $380 W \cdot m^{-1} \cdot K^{-1}$ for FeCrAl and copper, respectively and ε_F is the porosity of the foam.

The second term in Eq. (18) requires instead additional explanations. The heat transfer between the foam and the fluid/particle pseudo-phase takes place at the surface of the foam, $S_{V,F}$, calculated with the model of Ambrosetti and co-authors [39]. The overall heat transfer coefficient, instead, is referred to the internal surface of the reactor tube, thus a $4/d_t/S_{V,F}$ correction is needed. In our model, $U_{F \rightarrow PB}$ represents the overall heat transfer coefficient of a pseudo-channel with a diameter equal to the cell size of the foam, which is filled with catalyst particles and flowing gas. Therefore, engineering correlations suitable for the quantification of the overall heat transfer coefficients in channels with small tube to particle ratio can be adopted. In this work, $k_{eff,int}$ and $h_{w,int}$ were computed with the model of Specchia and co-workers (Eqs. (8)–(10)) [40], by using the foam cell size, d_{cell} , as the equivalent channel diameter. The overall heat transfer of the channel ($U_{F \rightarrow PB}$) was finally computed with the correlation proposed by Dixon [46]:

$$U_{F \rightarrow PB} = \left(\frac{1}{h_{w,int}} + \frac{d_{cell}}{a \cdot k_{eff,int}} \right)^{-1} \quad (20)$$

$$a = 6 \frac{Bi + 4}{Bi + 3} \quad (21)$$

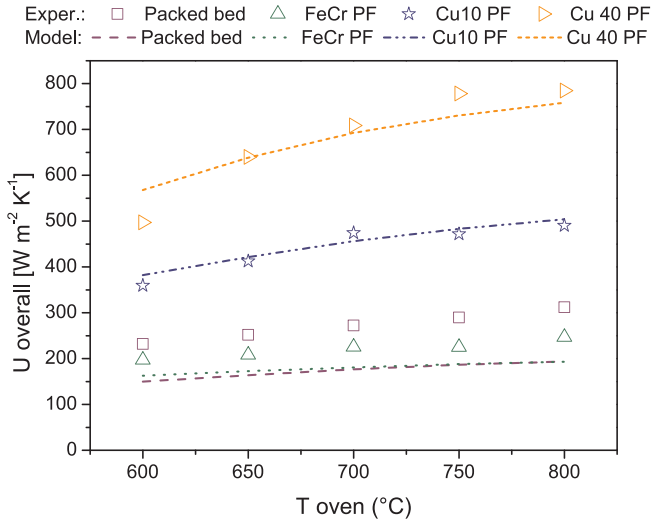


Fig. 10. Overall heat transfer coefficient as a function of oven temperature: model predictions and experimental results.

$$Bi = \frac{h_{w,int} d_{cell}}{2 \cdot k_{eff,int}} \quad (22)$$

According to the equations reported so far, $U_{overall}$ can be calculated according to the geometric and fluid-dynamic properties of the system. In these calculations, T was assumed equal to the temperature measured at the end of the catalytic bed by the thermocouple placed at 8 mm from the center of the reactor; the flow composition was assumed equal to the outlet stream composition.

3.5.3. Comparison with experimental results

Fig. 10 compares overall heat transfer coefficients predicted by Eqs. (6)–(22) (curves) and estimated from experimental results (symbols).

Generally speaking, a good accordance between experimental estimates and model predictions is apparent, which may suggest that the proposed equivalent circuit, although simplified, provides a representative description of the heat transfer phenomena in the reactor, correctly accounting for the physical evidence obtained from the experiments. It is noted in particular that the proposed heat transfer model provides a satisfactory prediction of the substantial equivalence between FeCr12 PF and SiC-diluted PB, of the remarkable improvement of heat transfer associated with the Cu10 PF and Cu40 PF configurations, as well as of the significant dependence of $U_{overall}$ on T /composition changes, which can be mainly attributed to the variation of the gas thermal conductivity.

On the basis of the equivalent circuit in Fig. 9, it was attempted to identify the contribution of each resistance to the overall heat transfer coefficient. Results are plotted in Fig. 11 in terms of conductances. Accordingly, the dominant term is the largest bar for in-parallel resistances and the smallest bar for the in-series ones.

The histograms in Fig. 11a show the internal resistance associated with the conductive heat transfer to be the limiting term for both the PB and the FeCr12 configurations. On the contrary, copper-based systems are characterized by higher internal conductances with respect to the wall conductances; this identifies the wall-to-foam coupling as the limiting factor for the overall system performance. The increased internal conductance is due to the improved heat transfer properties granted by the highly conductive internals.

Fig. 11b details the contribution of each circuitual element. In the packed bed configuration, due to the absence of the metallic foam, only two contributions are present. In the case of the FeCr12 packed foam, the poorly conductive matrix provides a minor contribution to the internal conductance; moreover a significant decrease of the term associated with the packed bed is due to the change of the dilution media,

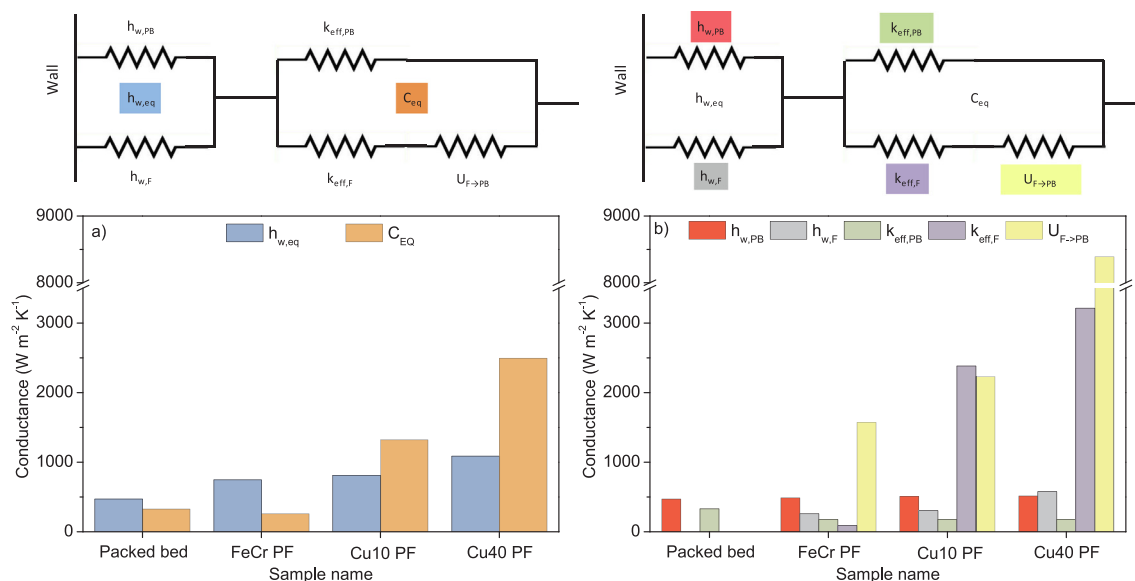


Fig. 11. Graphical representation of the contribution of each circuital component as a function of the reactor configuration (oven temperature and GHSV equal to 800 °C and 10,000 h⁻¹, respectively).

from the conductive SiC granules used for the PB tests to inert alumina particles used in the PF experiments. Accordingly, the overall heat transfer coefficient is not improved despite the presence of the foam and a significant enhancement of the wall heat transfer coefficient. Moving to copper foams, the high conductivity of the matrix significantly enhances the internal conductance. In the case of the Cu10 packed foam the internal foam to particle heat transfer plays some role, making the overall internal conductance almost equivalent to the wall conductance. Finally, in the Cu40 packed foam the effective conductivity of the copper matrix further increases due to the higher relative density (0.12 vs 0.09). More importantly, the foam to particle resistance becomes negligible due to the large increase of $S_{V,F}$ and the wall heat transfer coefficient, which is now the dominant contribution, significantly grows (from 812 to 1088 W·m⁻²·K⁻¹ for Cu10PF and Cu40PF, respectively) due to the smaller effective gap (Eq. (13), possibly associated with an increased number of foam-tube contact points. This results in an outstanding overall heat transfer coefficient of 750 W·m⁻²·K⁻¹. The analysis suggests that dedicated wall coupling strategies, such as the adoption of a foam soldered with an external skin, may further improve the wall coupling, minimizing the physical gap between the skin and the reactor tube and therefore improving the overall heat supply to the process.

4. Conclusions

The increasing interest in the development of compact methane steam reforming reactors for a distributed hydrogen economy calls for novel catalytic reactors with intensified heat management, which is the limiting factor of the current process technology. Conductive structured reactors have been reported as a valuable general strategy to enhance the performance of non-adiabatic processes by adopting washcoated metallic supports. However, washcoated structured reactors are affected by several limitations. Thus, in this work, the novel conductive packed foam configuration was studied for the intensification of steam methane reforming. In particular, copper packed foams were systematically investigated for the first time as efficient reactor internals. A lab scale proof of concept of the potential of the packed foam reactor configuration in CH₄ steam reforming has been thus obtained. Comparative experiments showed significant improvements in terms of both temperature profiles and of methane conversion, resulting from the presence of the highly conductive and interconnected cellular

matrices. Copper matrices enable higher conversions and reduced temperature gradients, allowing operating the reformer with more flexibility and better thermal efficiency.

Overall heat transfer coefficients of about 600–800 W·m⁻²·K⁻¹ have been estimated for the best performing packed foam, which relies primarily on static conductive (and radiative) heat transfer mechanisms and strongly outperform performances of packed bed reactors in the same operating conditions.

Furthermore, a previously reported heat transfer model for packed foam systems has been improved by considering additional heat transfer resistances and validated against the present experimental results.

The model identifies the wall heat transfer as the dominant resistance. This provides the basis for the rationale design of packed foams systems with optimal heat transfer and thermal efficiency performances, which is of paramount importance to develop compact reactors for the valorization of small-scale methane sources as well as for distributed hydrogen production, e.g. in micro-combined units (micro-CHP), which promise to cogenerate heat and power for residential applications, or even in small-scale fuel processors for vehicular auxiliary power units (APUs).

Acknowledgement

The research leading to these results has received funding from the European Research Council under the European Union's Horizon 2020 research and innovation program (Grant Agreement no. 694910/INTENT).

Appendix A. Supplementary data

Supplementary data to this article can be found online at <https://doi.org/10.1016/j.cej.2019.123494>.

References

- [1] L. Baharudin, M.J. Watson, Hydrogen applications and research activities in its production routes through catalytic hydrocarbon conversion, *Rev. Chem. Eng.* 34 (2017) 43–72, <https://doi.org/10.1515/revce-2016-0040>.
- [2] O. Sanz, I. Velasco, I. Reyero, I. Legorburu, G. Arzamendi, Effect of the thermal conductivity of metallic monoliths on methanol steam reforming, *Catal. Today* 273 (2016) 131–139, <https://doi.org/10.1016/j.cattod.2016.03.008>.
- [3] S. Specchia, Fuel processing activities at European level: a panoramic overview, *Int.*

- J. Hydrogen Energy 39 (2014) 17953–17968, <https://doi.org/10.1016/j.ijhydene.2014.04.040>.
- [4] G. Kolb, Review: microstructured reactors for distributed and renewable production of fuels and electrical energy, *Chem. Eng. Process. Process Intensif.* 65 (2013) 1–44, <https://doi.org/10.1016/j.ccep.2012.10.015>.
- [5] S. Ahmed, M. Krumpelt, Hydrogen from hydrocarbon fuels for fuel cells, *Int. J. Hydrogen Energy* 26 (2001) 291–301, [https://doi.org/10.1016/S0360-3199\(00\)00097-5](https://doi.org/10.1016/S0360-3199(00)00097-5).
- [6] J.-H. Ryu, K.-Y. Lee, H. La, H.-J. Kim, J.-I. Yang, H. Jung, Ni catalyst wash-coated on metal monolith with enhanced heat-transfer capability for steam reforming, *J. Power Sources* 171 (2007) 499–505, <https://doi.org/10.1016/j.jpowsour.2007.05.107>.
- [7] J. Gascon, J.R. van Ommen, J.A. Moulijn, F. Kapteijn, Structuring catalyst and reactor – an inviting avenue to process intensification, *Catal. Sci. Technol.* 5 (2015) 807–817, <https://doi.org/10.1039/C4CY01406E>.
- [8] L. Baharudin, M.J. Watson, Monolithic substrate support catalyst design considerations for steam methane reforming operation, *Rev. Chem. Eng.* 34 (2018) 481–501, <https://doi.org/10.1515/revce-2016-0048>.
- [9] A.K. Avci, D.L. Trimm, M. Karakaya, Microreactor catalytic combustion for chemicals processing, *Catal. Today* 155 (2010) 66–74, <https://doi.org/10.1016/j.cattod.2009.01.046>.
- [10] G. Kolb, V. Hessel, V. Cominos, H. Pennemann, J. Schürer, R. Zapf, H. Löwe, Microstructured fuel processors for fuel-cell applications, *J. Mater. Eng. Perform.* 15 (2006) 389–393, <https://doi.org/10.1361/105994906X117161>.
- [11] R.J. Farrauto, Y. Liu, W. Ruettinger, O. Ilinich, L. Shore, T. Giroux, Precious Metal Catalysts Supported on Ceramic and Metal Monolithic Structures for the Hydrogen Economy, *Catal. Rev.* 49 (2007) 141–196, <https://doi.org/10.1080/01614940701220496>.
- [12] E. Tronconi, G. Groppi, C.G. Visconti, Structured catalysts for non-adiabatic applications, *Curr. Opin. Chem. Eng.* 5 (2014) 55–67, <https://doi.org/10.1016/j.coche.2014.04.003>.
- [13] A. Montebelli, C.G. Visconti, G. Groppi, E. Tronconi, C. Cristiani, C. Ferreira, S. Kohler, Methods for the catalytic activation of metallic structured substrates, *Catal. Sci. Technol.* 4 (2014) 2846–2870, <https://doi.org/10.1039/c4cy00179f>.
- [14] L. Sang, B. Sun, H. Tan, C. Du, Y. Wu, C. Ma, Catalytic reforming of methane with CO₂ over metal foam based monolithic catalysts, *Int. J. Hydrogen Energy* 37 (2012) 13037–13043, <https://doi.org/10.1016/j.ijhydene.2012.05.056>.
- [15] H. Yu, H. Chen, M. Pan, Y. Tang, K. Zeng, F. Peng, H. Wang, Effect of the metal foam materials on the performance of methanol steam micro-reformer for fuel cells, *Appl. Catal. A Gen.* 327 (2007) 106–113, <https://doi.org/10.1016/j.apcata.2007.05.003>.
- [16] P.S. Roy, N.-K. Park, K. Kim, Metal foam-supported Pd-Rh catalyst for steam methane reforming and its application to SOFC fuel processing, *Int. J. Hydrogen Energy* 39 (2014) 4299–4310, <https://doi.org/10.1016/j.ijhydene.2014.01.004>.
- [17] P.S. Roy, A.S.K. Raju, K. Kim, Influence of S/C ratio and temperature on steam reforming of model biogas over a metal-foam-coated Pd-Rh/(CeZrO₂-Al₂O₃) catalyst, *Fuel* 139 (2015) 314–320, <https://doi.org/10.1016/j.fuel.2014.08.062>.
- [18] F.J. Echave, O. Sanz, I. Velasco, J.A. Odriozola, M. Montes, Effect of the alloy on micro-structured reactors for methanol steam reforming, *Catal. Today* 213 (2013) 145–154, <https://doi.org/10.1016/j.cattod.2013.02.027>.
- [19] V. Palma, D. Pisano, M. Martino, P. Ciambelli, Structured catalysts with high thermoconductive properties for the intensification of Water Gas Shift process, *Chem. Eng. J.* 304 (2016) 544–551, <https://doi.org/10.1016/j.cej.2016.06.117>.
- [20] D. Park, D.J. Moon, T. Kim, Preparation and evaluation of a metallic foam catalyst for steam-CO₂ reforming of methane in GTL-FPSO process, *Fuel Process. Technol.* 124 (2014) 97–103, <https://doi.org/10.1016/j.fuproc.2014.02.021>.
- [21] D. Park, D.J. Moon, T. Kim, Steam-CO₂ reforming of methane on Ni/γ-Al₂O₃-deposited metallic foam catalyst for GTL-FPSO process, *Fuel Process. Technol.* 112 (2013) 28–34, <https://doi.org/10.1016/j.fuproc.2013.02.016>.
- [22] H. Yang, J. Li, H. Yu, F. Peng, H. Wang, Metal-foam-supported Pd/Al₂O₃ catalysts for catalytic combustion of methane: effect of interaction between support and catalyst, *Int. J. Chem. React. Eng.* 13 (2015) 83–93, <https://doi.org/10.1515/ijcre-2014-0009>.
- [23] W. Zhou, Y. Ke, Q. Wang, S. Wan, J. Lin, J. Zhang, K.S. Hui, Development of cylindrical laminated methanol steam reforming microreactor with cascading metal foams as catalyst support, *Fuel* 191 (2017) 46–53, <https://doi.org/10.1016/j.fuel.2016.11.058>.
- [24] C.C. Shen, T.Y. Jian, Y.T. Wang, Steam reforming of methanol in a compact copper microchannel foam reactor, *Fuel Cells* 13 (2013) 965–970, <https://doi.org/10.1002/face.201300169>.
- [25] S. Catillon, C. Louis, R. Rouget, Development of new Cu⁰-Zn^{II}/Al₂O₃ catalyst supported on copper metallic foam for the production of hydrogen by methanol steam reforming, *Top. Catal.* 30 (2004) 463–467, <https://doi.org/10.1023/B:TOCA.0000029838.42709.7c>.
- [26] J. Qi, Y. Sun, Z. Xie, M. Collins, H. Du, T. Xiong, Development of Cu foam-based Ni catalyst for solar thermal reforming of methane with carbon dioxide, *J. Energy Chem.* 24 (2015) 786–793, <https://doi.org/10.1016/j.jechem.2015.10.001>.
- [27] J.T. Jang, K.J. Yoon, G.Y. Han, Methane reforming and water splitting using zirconia-supported cerium oxide in a volumetric receiver-reactor with different types of foam devices, *Sol. Energy* 101 (2014) 29–39, <https://doi.org/10.1016/j.solener.2013.12.019>.
- [28] C.G. Visconti, G. Groppi, E. Tronconi, Highly conductive “packed foams”: a new concept for the intensification of strongly endo- and exo-thermic catalytic processes in compact tubular reactors, *Catal. Today* 273 (2015) 178–186, <https://doi.org/10.1016/j.cattod.2016.02.060>.
- [29] M. Ambrosetti, M. Bracconi, M. Maestri, G. Groppi, E. Tronconi, Packed foams for the intensification of catalytic processes: assessment of packing efficiency and pressure drop using a combined experimental and numerical approach, *Chem. Eng. J.* 382 (2020) 122801, <https://doi.org/10.1016/j.cej.2019.122801>.
- [30] L. Fratolocchi, C.G. Visconti, G. Groppi, L. Lietti, E. Tronconi, Intensifying heat transfer in Fischer-Tropsch tubular reactors through the adoption of conductive packed foams, *Chem. Eng. J.* 349 (2018) 829–837, <https://doi.org/10.1016/j.cej.2018.05.108>.
- [31] R. Balzarotti, A. Beretta, G. Groppi, E. Tronconi, A comparison between washcoated and packed copper foams for the intensification of methane steam reforming, *React. Chem. Eng.* 4 (2019) 1387–1392, <https://doi.org/10.1039/C9RE00125E>.
- [32] L. Kiewidt, J. Thöming, Pareto-optimal design and assessment of monolithic sponges as catalyst carriers for exothermic reactions, *Chem. Eng. J.* 359 (2019) 496–504, <https://doi.org/10.1016/j.cej.2018.11.109>.
- [33] A. Porta, L. Falbo, C.G. Visconti, L. Lietti, C. Bassano, P. Deiana, Synthesis of Ru-based catalysts for CO₂ methanation and experimental assessment of intraporous transport limitations, *Catal. Today* (2019), <https://doi.org/10.1016/j.cattod.2019.01.042>.
- [34] A. Beretta, A. Donazzi, G. Groppi, P. Forzatti, V. Dal Santo, L. Sordelli, V. De Grandi, R. Psaro, Testing in annular micro-reactor and characterization of supported Rh nanoparticles for the catalytic partial oxidation of methane: effect of the preparation procedure, *Appl. Catal. B Environ.* 83 (2008) 96–109, <https://doi.org/10.1016/j.apcatb.2008.02.007>.
- [35] E. Bianchi, T. Heidig, C.G. Visconti, G. Groppi, H. Freund, E. Tronconi, An appraisal of the heat transfer properties of metallic open-cell foams for strongly exo-/endothermic catalytic processes in tubular reactors, *Chem. Eng. J.* 198–199 (2012) 512–528, <https://doi.org/10.1016/j.cej.2012.05.045>.
- [36] C. Murkin, J. Brightling, Eighty years of steam reforming, *Johnson Matthey Technol. Rev.* 60 (2016) 263–269, <https://doi.org/10.1595/205651316X692923>.
- [37] A. Donazzi, A. Beretta, G. Groppi, P. Forzatti, Catalytic partial oxidation of methane over a 4% Rh/α-Al₂O₃ catalyst: Part I: kinetic study in annular reactor, *J. Catal.* 255 (2008) 241–258, <https://doi.org/10.1016/j.jcat.2008.02.009>.
- [38] A. Beretta, G. Groppi, C. Ribani, G. Fares, C. Tregambe, Development of a catalytic fuel processor for a 10 kW combined heat and power system: experimental and modeling analysis of the steam reforming unit, *ChemEng. J.* 2 (2018) 5, <https://doi.org/10.3390/chemengineering2010005>.
- [39] M. Ambrosetti, M. Bracconi, G. Groppi, E. Tronconi, Analytical geometrical model of open cell foams with detailed description of strut-node intersection, *Chem.-Ing.-Tech.* 89 (2017) 915–925, <https://doi.org/10.1002/cite.201600173>.
- [40] V. Specchia, G. Baldi, S. Sicardi, Heat transfer in packed bed reactors with one phase flow, *Chem. Eng. Commun.* 4 (1980) 361–380, <https://doi.org/10.1080/00986448008935916>.
- [41] P. Aghaei, C.G. Visconti, G. Groppi, E. Tronconi, Development of a heat transport model for open-cell metal foams with high cell densities, *Chem. Eng. J.* 321 (2017) 432–446, <https://doi.org/10.1016/j.cej.2017.03.112>.
- [42] VDI e.V., ed., VDI-Wärmeatlas, Springer Vieweg, Berlin, Heidelberg, 2013. doi: <https://doi.org/10.1007/978-3-642-19981-3>.
- [43] R.J. Berger, EUROKIN spreadsheet on requirements for measurement of intrinsic kinetics in the gas-solid fixed bed reactor, in: 2012. <https://eurokin.org/>.
- [44] J.E. Crider, A.S. Foss, Effective wall heat transfer coefficients and thermal resistances in mathematical models of packed beds, *AIChE J.* 11 (1965) 1012–1019, <https://doi.org/10.1002/aic.690110613>.
- [45] M. Bracconi, M. Ambrosetti, M. Maestri, G. Groppi, E. Tronconi, A fundamental analysis of the influence of the geometrical properties on the effective thermal conductivity of open-cell foams, *Chem. Eng. Process. - Process Intensif.* 129 (2018) 181–189, <https://doi.org/10.1016/j.ccep.2018.04.018>.
- [46] A.G. Dixon, An improved equation for the overall heat transfer coefficient in packed beds, *Chem. Eng. Process. Process Intensif.* 35 (1996) 323–331, [https://doi.org/10.1016/0255-2701\(96\)80012-2](https://doi.org/10.1016/0255-2701(96)80012-2).